

# A simplified model design of MMC-HVDC transmission system for steady state and transient stability analyses

Marwan Rosyadi<sup>1</sup>, Atsushi Umemura<sup>2</sup>, Rion Takahashi<sup>2</sup>, Junji Tamura<sup>2</sup>,  
Takanori Uchiumi<sup>3</sup>, Masanori Mori<sup>3</sup>, Hiroki Miyata<sup>3</sup>

<sup>1</sup>Department of Electrical Engineering, Universitas Muhammadiyah Surabaya, Surabaya, Indonesia

<sup>2</sup>Department of Electrical and Electronic Engineering, Kitami Institute of technology, Kitami, Japan

<sup>3</sup>Department Engineering, Hokkaido Electric Power Network Inc, Sapporo, Japan

## Article Info

### Article history:

Received Oct 14, 2022

Revised Dec 12, 2022

Accepted Dec 27, 2022

### Keywords:

HVDC transmission system  
Modular multi-level converter  
Simplified modeling  
Steady state analysis  
Transient analysis

## ABSTRACT

A simplified model of a modular multilevel converter (MMC) implemented on a high voltage direct current (HVDC) transmission system is presented in this study for the analyses of steady-state and transient stabilities. The simplified model design's goal is to reduce the complicated modeling of the MMC circuit as well as the simulation time of the analysis. The validity of the model design has been examined using the PSCAD/EMTDC simulation program, where the simulation outcomes of the detailed model and the simplified model are contrasted. It has been established that the simplified model is accurate enough and that simulation time can be substantially decreased. It is concluded that the suggested model design is very significant as a simplified model for analyzing the steady state and transient stabilities of MMC-HVDC transmission system.

*This is an open access article under the [CC BY-SA](https://creativecommons.org/licenses/by-sa/4.0/) license.*



## Corresponding Author:

Marwan Rosyadi

Department of Electrical Engineering, Universitas Muhammadiyah Surabaya

Raya Sutorejo St. No. 59, Sutorejo, Mulyorejo, Surabaya, East Java, 60113, Indonesia

Email: rosyadi@um-surabaya.ac.id

## 1. INTRODUCTION

The increasing need for solving the global warming and a deregulated electricity market has brought about the penetration of high capacity of power plant sourced from renewable energy into grid systems such as wind farm based offshore system, in which a high-voltage transmission system is needed which should be more efficient, more inexpensive, more robust, and controllable. In addition, the transmission system is required to be able to cope with large power fluctuations without losing its stability. For overcoming those problems, the HVDC transmission system becomes an answer to meet the needs of transferring large amounts of electrical energy safely and reliably. HVDC transmission system is at lower cost than high voltage alternating current (HVAC) system above break-even distance [1]. In Europe, for example, HVDC transmission systems based on MMC technology have been widely used in offshore wind farms connected to onshore grids via long transmission cables [2]–[5]. The new Hokkaido-Honshu HVDC Link, an MMC-based HVDC interconnection line, has recently begun operation in Japan as well [6], [7].

The modular multilevel converter (MMC) is a novel converter concept designed for medium and high voltage applications in HVDC technology [8], [9]. The MMC has numerous advantages over conventional converters such as two or three levels converter, that is, high efficiency, good quality of voltage and current outputs, modularity and scalability, and small capacity of DC capacitors [10]. Therefore, the HVDC transmission with MMC system has been receiving considerable attention from engineers in the academic and industrial recently.

Power system stability analysis is particularly important in power system design. Simulation study of the MMC system with detailed model representations performed by using e.g., PSCAD/EMTDC or MATLAB/Simulink becomes incredibly challenging because the need to include numerous sub-modules (SMs) based insulated gate bipolar transistors (IGBTs) in the simulation study. In the case of trans bay HVDC cable project with  $\pm 200$  kV DC transmission voltage rating, which is the first HVDC system using MMC system, its converter system is configured by 201 levels of MMC. The MMC requires around 2400 IGBTs with anti-parallel diodes and 1200 sub-module capacitors which are connected electrically [11]. Simulation studies by using such detailed model may become inefficient. Therefore, the dynamic behavior analysis of MMC-HVDC transmission system should be represented by standard simplified model which is suitable for simulating the time domain instantaneous responses.

The efforts to simplify MMC-HVDC transmission system have been reported in some papers [12]–[15]. The simplified models are based on phasor model approach and are represented as two level or three levels converter with small modification. The fast and simultaneous simulation method for the MMC-HVDC transmission system was implemented to decrease the computational time for transient analysis [16]. In the method, the large sized admittance matrix including many nodes of the MMC part in the detailed model is modeled into a simple electrical equivalent circuit by using Thevenin or Norton theorems. However, this method still needs to simplify the overly complex admittance matrix. The other simplification approaches such as equivalent circuit model, MMC switching function model, detailed nonlinear IGBT model, and the average value model (AVM) for dynamic performance analysis are presented in some papers [17]–[19]. The AVM approach can reduce the computation time significantly. However, at least 40  $\mu$ s of simulation time step is needed to get sufficient accuracy [18].

In the previous work, simplification of MMC circuit has been developed in the average model for permanent magnet wind turbine generator [20]. The MMC system is implemented on the converters (rectifier and inverter) of the wind generator. The designed average model of the wind generator, however, cannot be directly applied to the MMC-HVDC transmission system model. Therefore, a novel approach is required for developing a simplified model of the MMC-HVDC transmission system.

In this study, a simplified model design for MMC-HVDC transmission system is proposed. The SMs-based IGBT is not explicitly modeled in the MMC circuit in the model design; instead, the MMC circuit is only represented by sources of voltage and current. Therefore, large time step (100  $\mu$ s) of simulation can be used. In addition, the model does not require complex mathematical simplification. Moreover, one of the advantages of this simplified model is that it can be easily applied to electromagnetic transient simulation analyses on standard software such as PSCAD/EMTDC or MATLAB/Simulink. One thing to keep in mind is that the simplified model is meant to be an alternative model to the simpler models that have been created.

## 2. HVDC TRANSMISSION SYSTEM MODEL

Figure 1 illustrates the power system model used in this study for the simulation, which is a two-connected areas power system with an HVDC transmission system. Two independent AC power systems are connected through a 200 MVA ( $\pm 100$  kV) symmetrical monopolar HVDC transmission line. The HVDC transmission line is used to transfer electric power from Area 1 to Area 2. Both the rectifier station and the inverter station utilize the MMC system, which connects them via A 75-kilometer power cables. The  $\pi$  equivalent circuit model represents the power cable.

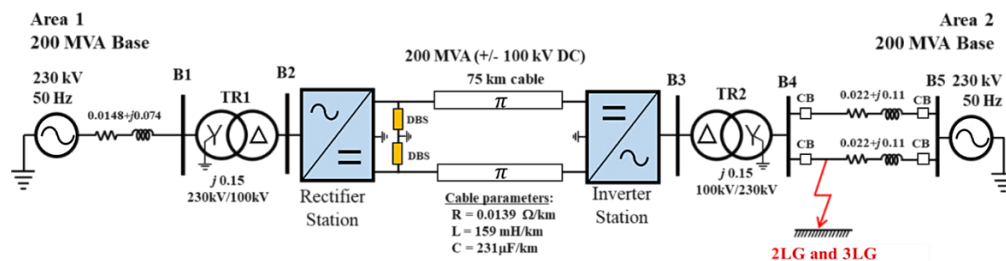


Figure 1. Two power systems connected by MMC-HVDC transmission line model

Two dynamic braking systems (DBSs) are installed in DC output terminal of MMC circuit of the inverter. The rectifier station is connected to Area 1 through a 230 kV/100 kV rectifier transformer (TR1) and single circuit of transmission line. On the other hand, the inverter station is linked to Area 2 via a 100 kV/230 kV inverter transformer (TR2) and 230 kV transmission lines. The transmission lines are designed with two circuits. The parameters of transmission line are written in  $R+jX$  form, where  $R$  represents

the resistance and  $X$  the reactance. The parameters of the MMC are presented in Table 1. The operating mechanism of the rectifier station is to transform the voltage from AC to DC forms. Furthermore, the rectifier station also regulates the active power flow from Area 1 into the HVDC transmission circuit. On the other hand, the inverter station transforms the voltage from DC to AC forms. The inverter station works to maintain the HVDC transmission's DC voltage at its rated voltage, which enables active power from Area 1 to be delivered to Area 2. The reactive power output, which is constrained by the converters' capacity, can be independently adjusted by the rectifier and inverter (PQ diagram of converter).

Table 1. Parameters of modular multilevel converter

Parameter	Value	Unit	Parameter	Value	Unit
Power	200	MVA	Arm inductor	15.9	mH
AC voltage	100	kV	Arm resistor	0.05	$\Omega$
AC frequency	50	Hz	Reactor inductance	15.9	mH
DC voltage	$\pm 100$	kV	Reactor resistance	0.05	$\Omega$
SM per arm	8	module	DC capacitor	1750	$\mu\text{F}$
SM capacitor	3400	$\mu\text{F}$			

### 3. DETAILED MODEL OF MMC SYSTEM

As previously stated, performing a simulation study for the MMC based on its detailed model in real configuration is extremely difficult, as hundreds of sub-modules must be considered. Therefore, the detailed model of the MMC in the power system illustrated in Figure 1 is represented by nine levels of MMC system. In the converter stations, the MMC system is made up of 48 sub-modules (96 IGBTs with antiparallel diodes and 48 sub-module capacitors).

#### 3.1. Configuration of MMC circuit

The MMC configuration in three phase topologies is shown in Figure 2. Each phase has a phase leg, which is made up of two-phase arms. The phase arm has 8 sub-modules ( $SM_{U1...8}$  for upper arm and  $SM_{L1...8}$  for lower arm), arm resistance ( $R_{arm}$ ), and arm inductor ( $L_{arm}$ ). The arm inductors serve as an interface impedance between the AC grid system and the MMC circuit, and serve for limiting the circulating arm current between the valve and phase legs [21]. The sub-module is of half bridge type configuration which consists of two IGBTs and a sub-module capacitor ( $C_{SM}$ ). The two antiparallel diodes are installed in parallel with the IGBTs. Point of connection between the upper and the lower arms is linked to the MMC AC terminal by filter inductance ( $L_f$ ) and resistance ( $R_f$ ). The filter can reduce the current and voltage ripples of the AC side output. Each terminal end of upper arms and lower arms is connected to each other, and respectively become positive (+) and negative (-) output terminal of DC circuit. The DC capacitors ( $C_{dc}$ ) are installed on the DC circuit for reducing the DC voltage ripple.

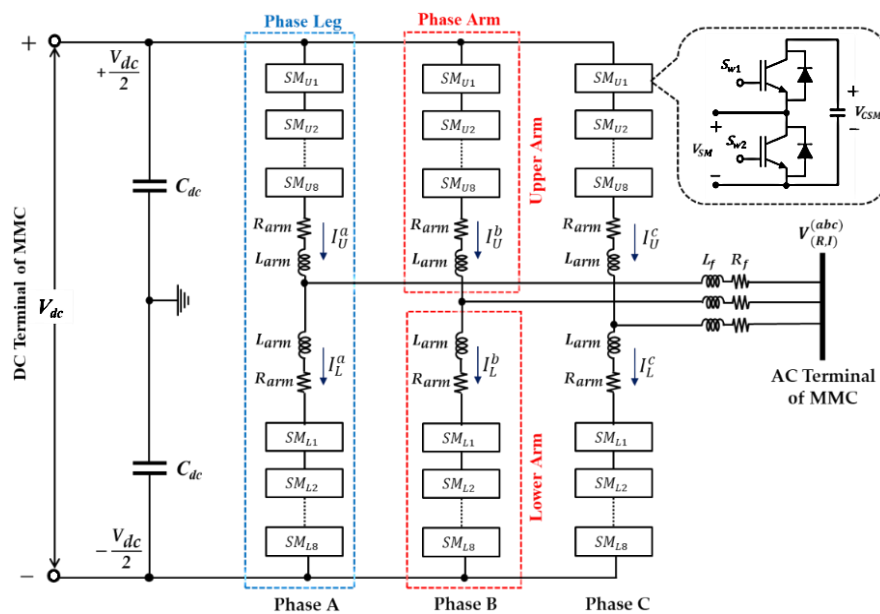


Figure 2. Configuration of the 9-levels circuit MMC in three phase topologies

In operating of MMC circuit, the DC voltage ( $V_{dc}$ ) is distributed to entire sub-module capacitor ( $C_{SM}$ ). Then, the sub-module capacitor status consistently becomes charging and discharging according to the operating mode of the IGBTs switching state and current arm polarities. Sub-module capacitor status in detail can be seen in Table 2.

Table 2. Operating condition of sub-module based on switching state

Switching State		Arm Current Polarity	Terminal Voltage of Sub-Module	Sub-Module Capacitor Status
$Sw1$	$Sw2$			
ON	OFF	+	$V_{CSM}$	Charge
OFF	ON	+	0	Bypass
ON	OFF	-	$V_{CSM}$	Discharge
OFF	ON	-	0	Bypass

### 3.2. Control mechanism of the MMC

Numerous publications containing modeling designs and control techniques for the MMC-HVDC Transmission system have been reported [21]–[27]. Figure 3 presents the control scheme commonly used in MMC-based HVDC systems. Voltage source converters (VSCs) connect two independent AC power systems, allowing both converter stations to control the active power. One of the converters, however, should be used to control the HVDC transmission line voltage. In this work, the inverter station regulates the voltage on the HVDC transmission line while the rectifier station controls the active power. Each converter has the ability to independently regulate the reactive power output.

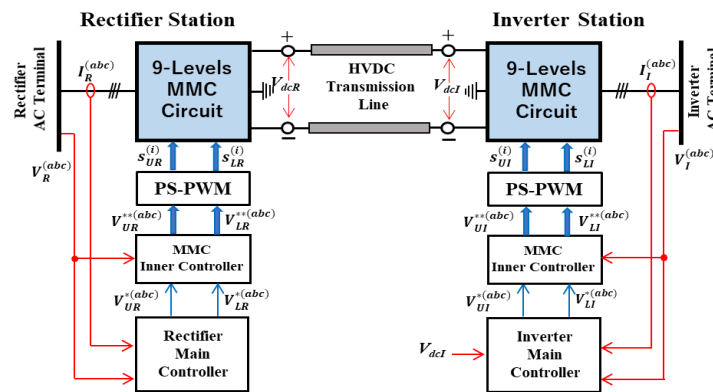


Figure 3. Control scheme of MMC based HVDC

Three-phase current and voltage at AC output terminal of the rectifier and the inverter ( $I_{(R,I)}^{(abc)}$ ,  $V_{(R,I)}^{(abc)}$ ) are fed to each main controller. Then, the main controllers control the three-phase reference voltage for each phase arm ( $V_{U(R,I)}^{*(abc)}$  and  $V_{L(R,I)}^{*(abc)}$ ) of the MMC circuit. In three-phase MMC circuit, a circulating current can occur on the phase legs. Moreover, the voltage level difference between sub-modules on upper and lower phase arms also can occur which can cause unbalance voltage on the sub-module capacitor [2]. The inner controller of MMC is introduced in the controller schemes for solving this problem. The new three phase voltages as references for modulating ( $V_{U(R,I)}^{**(abc)}$  and  $V_{L(R,I)}^{**(abc)}$ ) are obtained from the MMC inner controller. For the modulation technique, the multicarrier-based phase shifted pulse width modulation (PS-PWM) is implemented. The PS-PWM technique generates the PWM signals  $Sw_{U(R,I)}^{(i)}$  and  $Sw_{L(R,I)}^{(i)}$  to trigger the IGBT's gates of the sub-modules in the MMC circuit.

Figures 4 and 5 show the main controllers for the rectifier and inverter, respectively. The vector control method-based conventional VSC is used for the control loop strategy for rectifier and inverter [2]. For this purpose, by using Park Transformation three-phase voltage and current from the MMC AC terminal output are converted into the  $dq$ -axis form. The phase angles of grid voltage ( $\theta_R$  or  $\theta_I$ ) are detected by using phase locked loop (PLL) controller. It should be noted that the original block set models of the park transformation equation and the PLL technique available on the master library of PSCAD/EMTDC is used in this study [28]. The power meter calculates the instantaneous powers and the three phase rms voltmeter measures the rms voltage from the MMC AC terminal output. The parameters fed to the converter controllers are in per unit (pu).

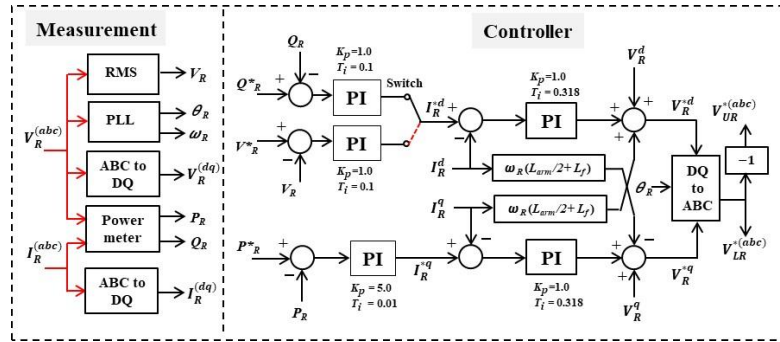


Figure 4. Rectifier main controller

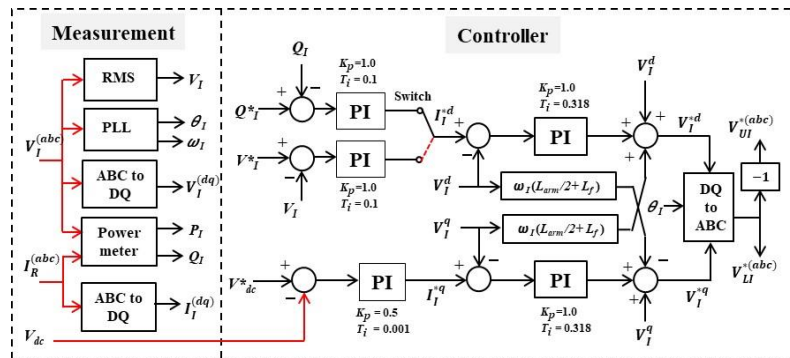


Figure 5. Inverter main controller

The inner current loop and outer power loop controllers of the MMC are made up of four PI controllers. In the rectifier main controller, the  $q$ -axis current ( $I_R^q$ ) controls the flow of active power ( $P_R$ ), while the  $d$ -axis current ( $I_R^d$ ) controls the reactive power ( $Q_R$ ) of the rectifier station. Under certain circumstances, the  $d$ -axis current can be chosen to regulate the voltage of the AC terminal rather than the reactive power. The references can be set to zero for reactive power ( $Q_R^*$ ) and 1.0 pu for AC voltage ( $V_R^*$ ). In the inverter main controller, the DC transmission line voltage ( $V_{dc}$ ) is maintained at rated voltage by controlling the inverter  $q$ -axis current ( $I_I^q$ ). The reactive power ( $Q_I$ ) or the AC terminal voltage ( $V_I$ ) of the inverter can be regulated through the inverter  $d$ -axis current ( $I_I^d$ ). The reactive power reference, like the rectifier controller mechanism, can be set to zero, or the reference voltage can be set to 1.0 pu. If the inverter AC voltage falls below 85% due to a short circuit, the inverter main controller switches from normal to fault mode. The inverter's main controller would switch from reactive power control to voltage control.

Figure 6 depicts the MMC inner controller. The MMC inner controller is implemented to the rectifier and the inverter stations. The MMC inner controller is made up of two SM capacitor voltage balancing controllers and a circulating current controller. The function of the circulating current controller is to prevent circulating current flows through the phase legs [29]. The circulating current ( $I_{cir}^{(abc)}$ ) can be calculated by summing the arm currents ( $I_U^{(abc)}$  and  $I_L^{(abc)}$ ) divided by two. The circulating current is converted into the  $d$ -axis and  $q$ -axis currents ( $I_{cir}^{(dq)}$ ), which are independently set to zero using PI controllers. The PI controllers adjust the circulation voltages ( $V_{cir}^{(dq)}$ ), which are then inverted into a three-phase voltage form ( $V_{cir}^{(abc)}$ ). The MMC inner controller produces new reference voltages  $V_U^{*(abc)}$  and  $V_L^{*(abc)}$  for upper and lower arms, respectively. To control voltage balancing of all capacitors, extra controllers must be installed throughout the SMs [30].

### 3.3. PS-PWM technique

The PS-PWM technique uses multiple triangle carrier signals along the horizontal axis with same frequency and voltage amplitude. The number of triangle carrier signal required is given by the number of levels of MMC ( $N$ ) minus one. Nine levels of MMC circuit requires eight triangle carrier signals. The generating pulse process of multi-carrier PS-PWM technique is shown in Figure 7. The phase shift ( $\phi$ ) of each carrier signal can be calculated as (1) [31].

$$\phi = 360^\circ / (N - 1) \tag{1}$$

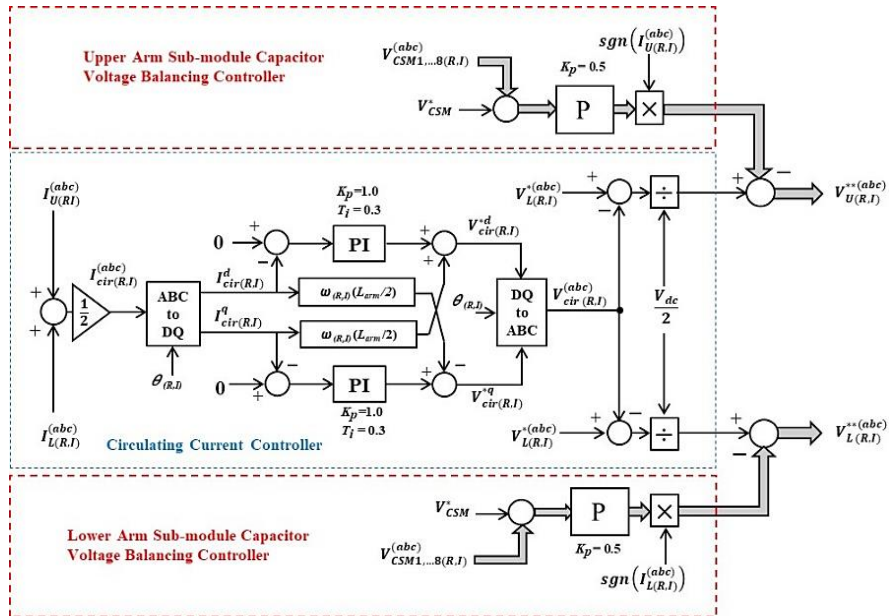


Figure 6. The MMC inner controller for rectifier station or inverter station

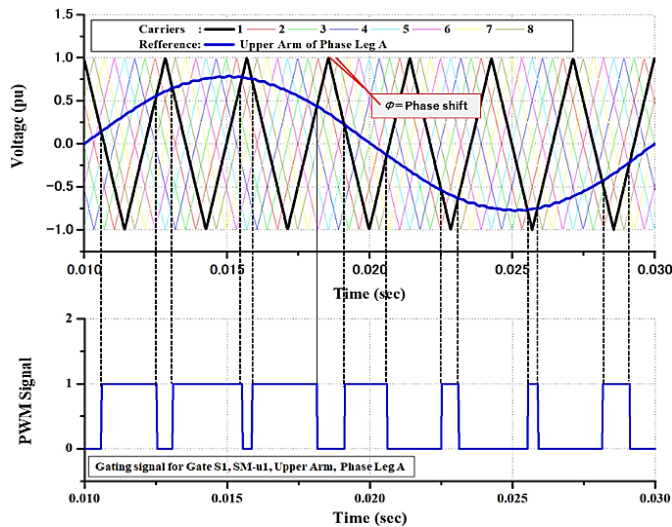


Figure 7. PS-PWM technique process

**3.4. Dynamic braking system (DBS)**

A DBS is installed across an HVDC transmission terminal to dissipate energy and limit transmission line overvoltage caused by transient disturbance on the AC grid system such as a short circuit. The DBS can help to increase capability of fault ride through (FRT) of HVDC system. According to IEC Standard 62747:2014, the DBS is recommended to be implemented in HVDC transmission system [32]. The DBS installation structure is determined by the type of HVDC system. Figure 8 depicts the basic structure of DBS that installed on symmetrical monopolar type of HVDC transmission system. The rectifier MMC circuit has two DBSs installed on the DC side. The DBS is composed of a group of semiconductors breaking valve and a breaking resistance ( $R_{dbs}$ ). The active power output of the inverter will abruptly decrease when there is a transient grid disturbance on the grid. Meanwhile, the rectifier station continues to supply active power to the HVDC circuit, and hence the power unbalance occurs between both stations. As consequence, the DC voltage on the transmission line increases significantly. The DBS will dissipate the active power in the braking resistance  $R_{dbs}$  by operating the semiconductor breaking valve (DBS valve). The DBS device is operated according to the HVDC voltage condition during a disturbance event. The DBS is executed when the HVDC transmission line voltage reaches the threshold limit (1.05 pu). The maximum value of  $R_{dbs}$  is selected according to nominal power rating of the HVDC link.

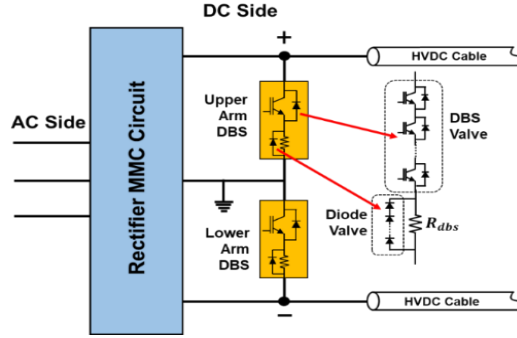


Figure 8. Basic structure of DBS on symmetrical monopolar HVDC transmission line

#### 4. SIMPLIFIED MODEL OF MM-HVDC TRANSMISSION SYSTEM

The equivalent approach model of a traditional voltage source converter (VSC) could be considered to represent the MMC-HVDC transmission system in a simplified model [33]. Figure 9 depicts the VSC equivalent model, in which three-phase voltage source and a current source connected to the AC and DC sides, respectively, represent the converter. The converter is connected to grid voltage sources ( $v_s^{(abc)}$ ) through phase reactor,  $L_f$  (reactor inductor) and  $R_f$  (reactor resistance). The voltage across the filter inductor for each phase can be using Kirchhoff voltage law (KVL):

$$L_f \frac{d}{dt} i_f^{(abc)} = v_s^{(abc)} - v_{con}^{(abc)} - R_f i_f^{(abc)} \quad (2)$$

where,  $v_{con}^{(abc)}$  is three phase terminal voltage of the converter.

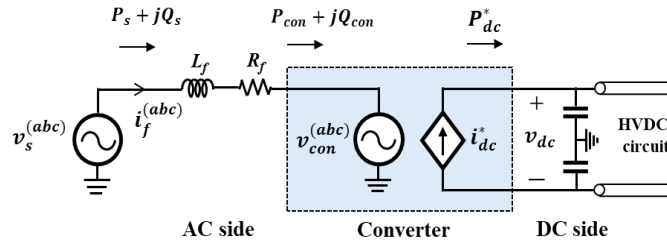


Figure 9. Equivalent model of VSC

The  $v_{con}^{(abc)}$  is equivalent to the three-phase voltage at the AC output terminal of the MMC circuit. Consider the electrical MMC circuit in the equivalent model in Figure 10 for more details. The  $v_{con}^{(abc)}$  can be regulated by the three phase arm voltages ( $v_U^{*(abc)}$ ) and ( $v_L^{*(abc)}$ ). The differential equations are obtained by applying KVL to both arm:

$$\frac{v_{dc}}{2} = v_{con}^{(abc)} + R_{arm} i_U^{(abc)} + L_{arm} \frac{di_U^{(abc)}}{dt} + v_U^{*(abc)} \quad (3)$$

$$\frac{v_{dc}}{2} = -v_{con}^{(abc)} + R_{arm} i_L^{(abc)} + L_{arm} \frac{di_L^{(abc)}}{dt} + v_L^{*(abc)} \quad (4)$$

from the figure, it is evident that:

$$i_f^{(abc)} = i_U^{(abc)} - i_L^{(abc)} \quad (5)$$

circulating current is defined as (6).

$$i_{cir}^{(abc)} = \frac{i_U^{(abc)} + i_L^{(abc)}}{2} \quad (6)$$

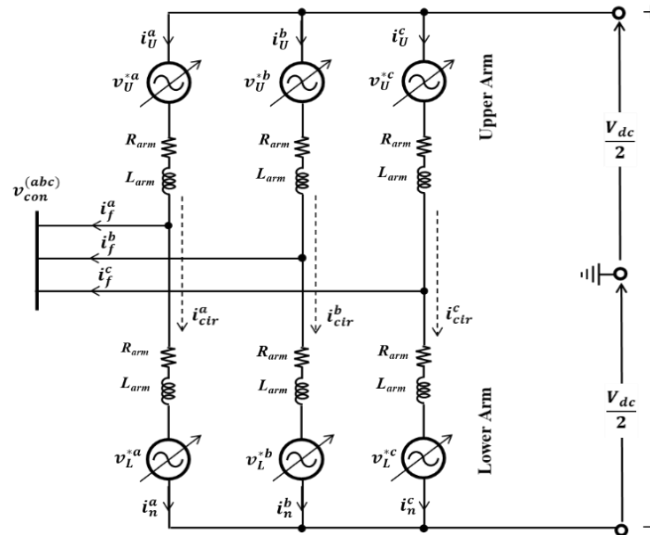


Figure 10. Equivalent of electrical MMC circuit

The voltage at the MMC terminal output is calculated using the (7).

$$v_{con}^{(abc)} = e^{(abc)} - \frac{L_{arm} di_f^{(abc)}}{2 dt} - R_{arm} i_f^{(abc)} \tag{7}$$

Where,  $e^{(abc)}$  is the inner emf of three phases, as (8).

$$e^{(abc)} = \frac{v_L^{*(abc)} - v_U^{*(abc)}}{2} \tag{8}$$

In (7), the  $v_{con}^{(abc)}$  can be controlled through emf  $e^{(abc)}$  adjustment components  $v_U^{*(abc)}$  and  $v_L^{*(abc)}$ .

Returning to Figure 9, in (2) could be in the  $dq0$  frame as (9) and (10).

$$L_f \frac{di_f^d}{dt} = v_s^d - R_f i_f^d - v_{con}^d + \omega_s L_f i_f^q \tag{9}$$

$$L_f \frac{di_f^q}{dt} = v_s^q - R_f i_f^q - v_{con}^q - \omega_s L_f i_f^d \tag{10}$$

Where,  $\omega_s$  is angular frequency of the grid. The grid powers for both active and reactive in the complex form are as (11).

$$P_s + jQ_s = (v_s^d i_f^d + v_s^q i_f^q) + j(v_s^q i_f^d - v_s^d i_f^q) \tag{11}$$

The powers flow to the converter are also known as (12).

$$P_{con} + jQ_{con} = (v_{con}^d i_f^d + v_{con}^q i_f^q) + j(v_{con}^q i_f^d - v_{con}^d i_f^q) \tag{12}$$

In the steady state condition, the  $q$ -axis assumes to be in alignment with the vector  $\vec{v}_{con}^{(dq)}$ , thus the  $d$ -axis becomes zero, and the powers of the converter is as (13) and (14).

$$P_{con} = v_{con}^q i_f^q \tag{13}$$

$$Q_{con} = v_{con}^q i_f^d \tag{14}$$

Therefore, the  $q$ -axis current ( $i_f^q$ ) and the  $d$ -axis current ( $i_f^d$ ) could control independently the active and reactive powers.

The DC power ( $P_{dc}^*$ ) flows into the HVDC transmission line and is adjustable by injecting the DC current ( $i_{dc}^*$ ). Because reactive power has no effect on injected power to the DC side, the following relationship holds:



$$P_{dc}^* = P_{con} \Rightarrow v_{dc} i_{dc}^* = v_{con}^d i_f^d + v_{con}^q i_f^q \tag{15}$$

Finally, the dc current injected to the HVDC circuit can be calculated as (16).

$$i_{dc}^* = \frac{v_{con}^d i_f^d + v_{con}^q i_f^q}{v_{dc}} \tag{16}$$

To simplify the complicated MMC-HVDC transmission system model, IGBTs switching phenomena and modulation process in MMC rectifier and MMC inverter should be neglected in simulation analysis. Referring to Figures 9 and 10, a detailed scheme of the proposed simplified MMC-HVDC transmission system model is presented in Figure 11. The MMC circuit for a rectifier station or inverter station is made up of two electrical main circuits that are linked to the AC and DC side systems. The three-phase MMC arm circuit is made up of three-phase voltage sources, arm resistances, and arm inductors that are connected to the converters' AC terminals via the point of common connection. The DC voltage ( $V_{dc}/2$ ) powers the entire arm circuit. The three-phase voltage external input ( $V_{U(R,I)}^{*(abc)}$  and  $V_{L(R,I)}^{*(abc)}$ ) are obtained from the MMC main controller, and the DC voltage external input ( $\frac{V_{dc}}{2}$ ) is measured from the HVDC transmission line. A DC current source represents the MMC circuit for the interface to the DC side, and the external current input ( $i_{dc(R,I)}^*$ ) can be calculated using (15).

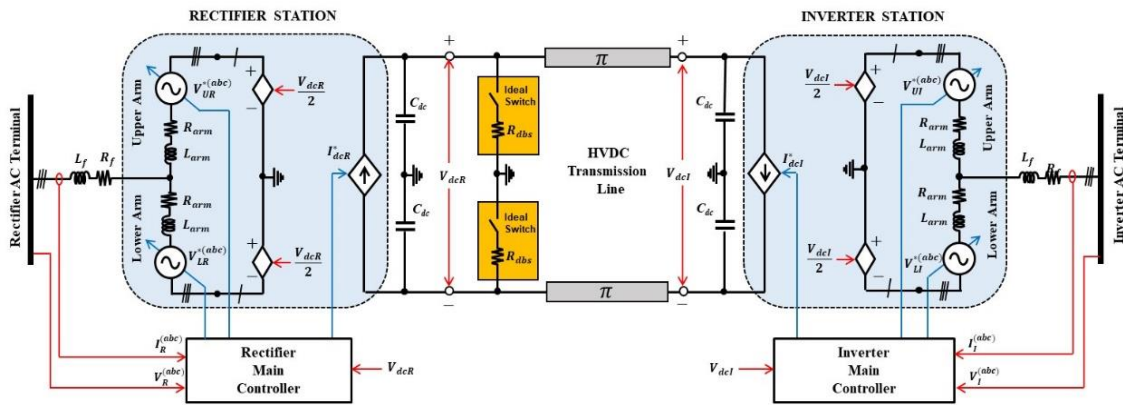


Figure 11. MMC-HVDC transmission system in simplified model

The main controller schemes and control methods for both the rectifier and inverter controllers in the detailed model can be applied also in the simplified model. Therefore, the rectifier and the inverter controllers presented in Figures 4 and 5 can also be used in the simplified model. In this study, the profile voltage of SM capacitor and profile circulation current on the phase leg in the proposed simplified model are assumed ideal. Therefore, the MMC inner controller is not considered. Furthermore, the steady-state and transient analyses focus on the profile voltage, current, and power output excursion on AC and DC sides of the MMC.

The transmission circuit of HVDC is configured by symmetrical monopolar type as well as the electrical topology in the detailed model. However, the DBSs which installed across the HVDC transmission line is represented by an ideal switch and a braking resistance for each arm. The switch is executed when the HVDC circuit voltage exceeds the voltage threshold, 1.05 pu.

## 5. SIMULATION STUDY

The model of two areas of the power system linked by the HVDC transmission line illustrated in Figure 1 is analyzed in the simulation study. The PSCAD/EMTDC software is used for the simulation study. The simulations were run on the PC (Intel i7-9700 CPU @3.0 GHz RAM 64 GB). A comparative responses analysis between the detailed and the simplified models was validated under steady-state and transient disturbances.

### 5.1. Simulation and analysis in steady state study

In this simulation study, the responses of terminal voltages and powers output of the HVDC transmission system during steady-state disturbance are analyzed. The simulation results are presented in Figures 12(a) to 12(f). For steady state disturbance, the up-down ramps and step changes in active power

reference are applied to the rectifier main controller as depicted in Figure 12(a). First, the up-ramp reference is gradually increased from 0.0 pu to 1.0 pu. Second, the step change reference is applied two times, at 5.0 sec from 1.0 pu to 0.8 pu, and at 7.0 sec from 0.8 pu to 1.0 pu. The down-ramp reference is activated at 9.0 sec, where the reference is gradually decreased from 1.0 pu to 0.0 pu.

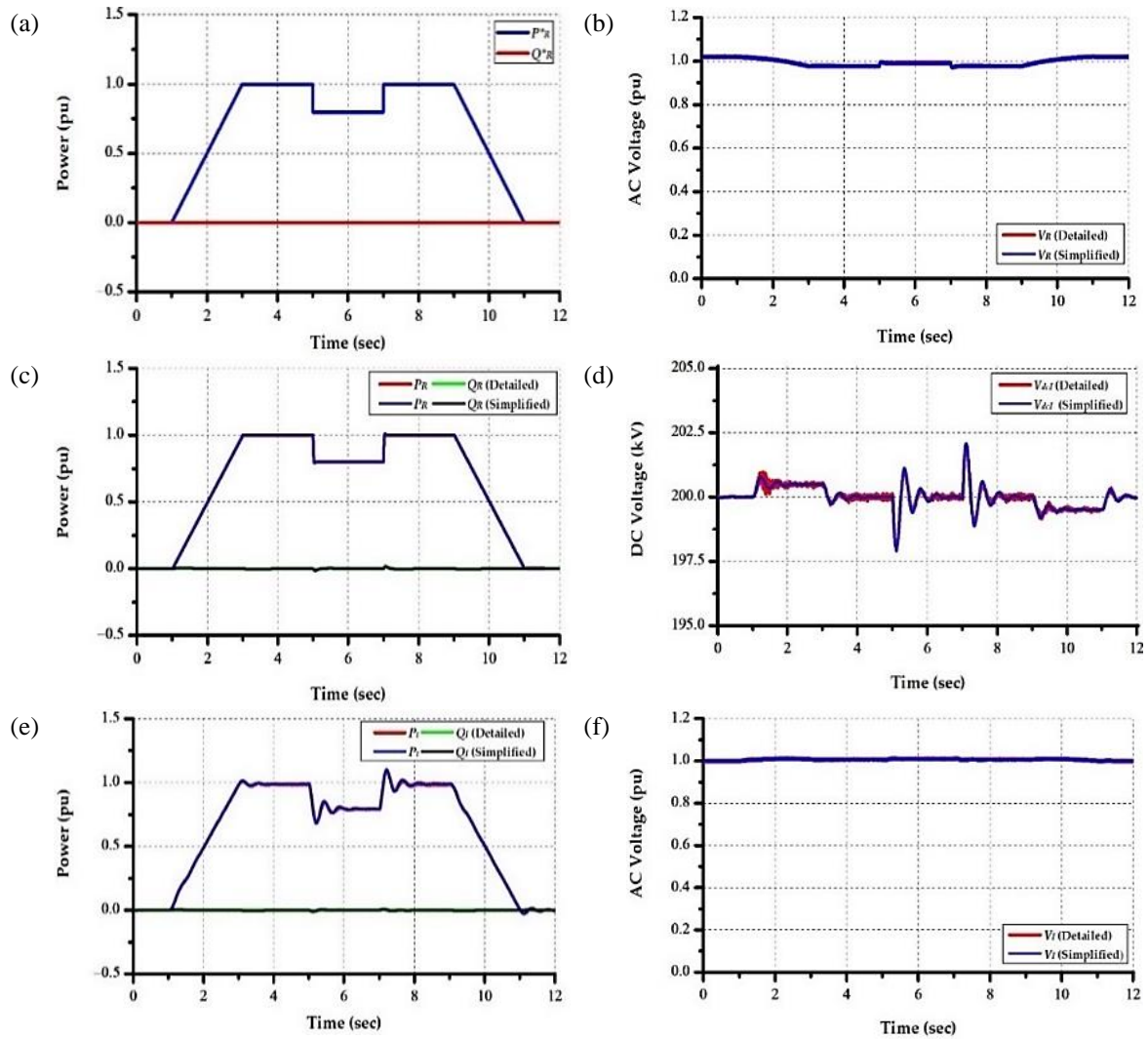


Figure 12. Simulation results in steady state condition: (a) active and reactive powers references, (b) AC voltage response at Bus B1, (c) active and reactive power responses at Bus B, (d) DC voltage response at the transmission line, (e) active and reactive power responses at Bus B4, and (f) AC voltage response at Bus B4

During the simulation, the reactive power of the converter stations is maintained to zero. According to the simulation results shown in Figures 12(b) to 12(f), the AC terminal voltage, the powers of both the converter stations, and the DC voltage of the transmission line of the simplified model have the same response as the detailed model. In the steady-state condition, the simplified model has adequate precision, which can be confirmed. In addition, as presented in Table 3 the simplified model can reduce simulation time more significantly compared to the simulation time obtained by the detailed model.

Table 3. Computation time for 12 sec simulation time

	Computation time	
	Simplified model	Detailed model
Simulation time step	100 $\mu$ s	10 $\mu$ s
Real time duration	7 seconds	70 minutes

**5.2. Simulation and analysis in transient study**

Asymmetrical two lines to ground fault (2LG) and symmetric three lines to ground fault (3LG) at the transmission line of Area 2 are regarded as network disturbances in the transient case study. Figure 1 depicts where the faults are located. Circuit breakers (CBs) on the faulted circuit are opened at 0.2 second following the occurrence of the fault at 0.1 second. The CBs are reclosed at 1.0 second under the presumption that the fault has been fixed.

The simulation results of the transient study for 2LG and 3LG are shown in Figures 13(a)-13(e) and Figures 14(a)-14(e) (see Appendix), respectively. According to the profile AC voltage, active and reactive power response at Bus B1, the faults (2LG or 3LG) in Area 2 had no effect on the Area 1. This is because, the DBS device can absorb the supplied active power from Area 1 when unbalanced power occurred between the inverter and the rectifier caused by the faults, hence the overvoltage on the HVDC transmission line can be well anticipated. The DC voltage responses are shown in Figures 13(c) and 14(c). Due to the voltage drop during the faults, the active power to Area 2 on Bus 4 abruptly decreased. After the faults are cleared, the active power can be restored to its original state. Meanwhile, the inverter supplies reactive power during the fault and returns to its original position once the fault is resolved. Based on the simulation results, the proposed simplified model of the MMC-HVDC transmission system has adequate precision in transient responses in the cases of 2LG and 3LG disturbances.

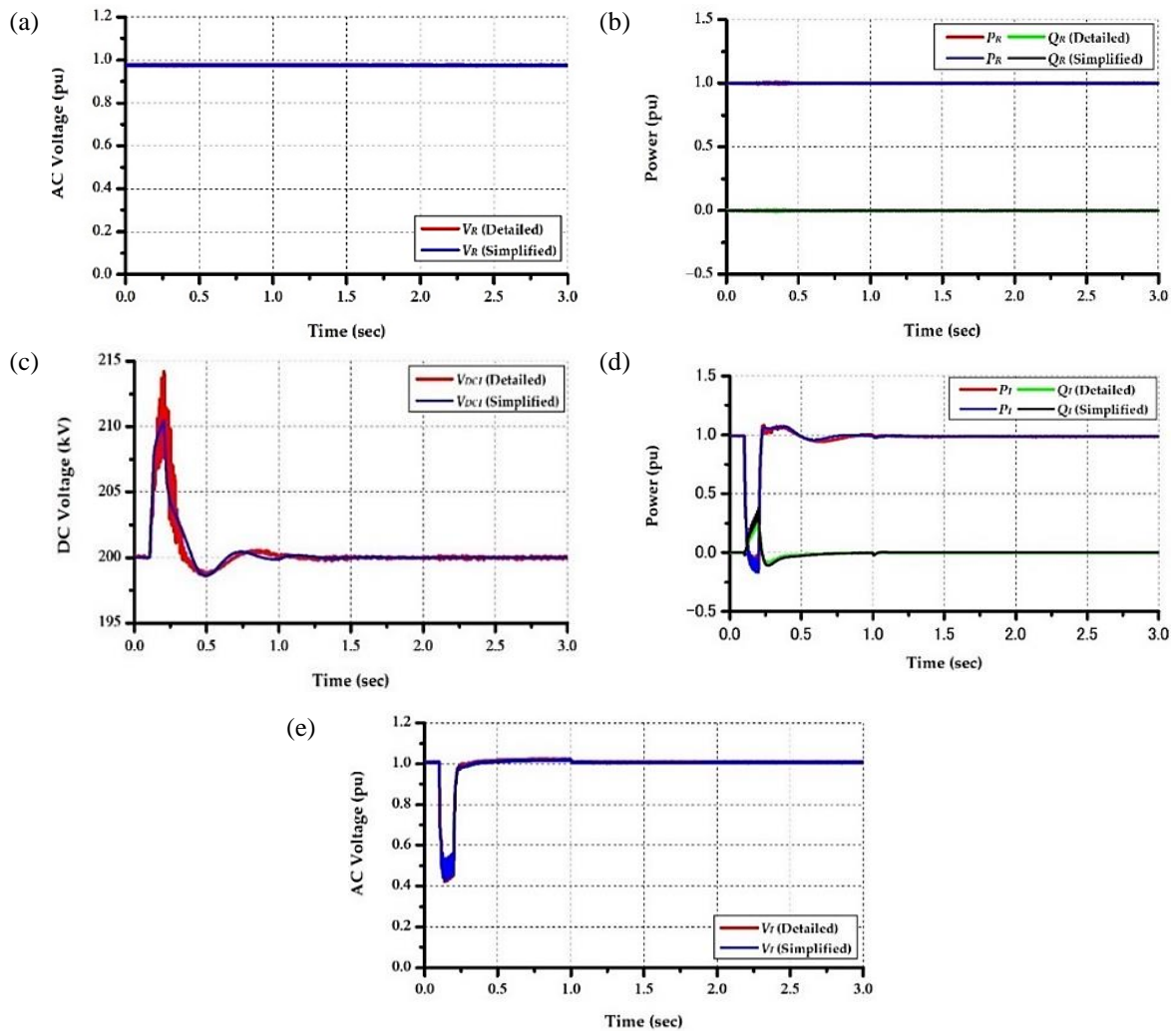


Figure 13. Simulation results of transient study for 2LG: (a) AC voltage response at Bus B1, (b) active and reactive power responses at Bus B1, (c) DC voltage response at the transmission line, (d) active and reactive power responses at Bus B4, and (e) AC voltage response at Bus B4

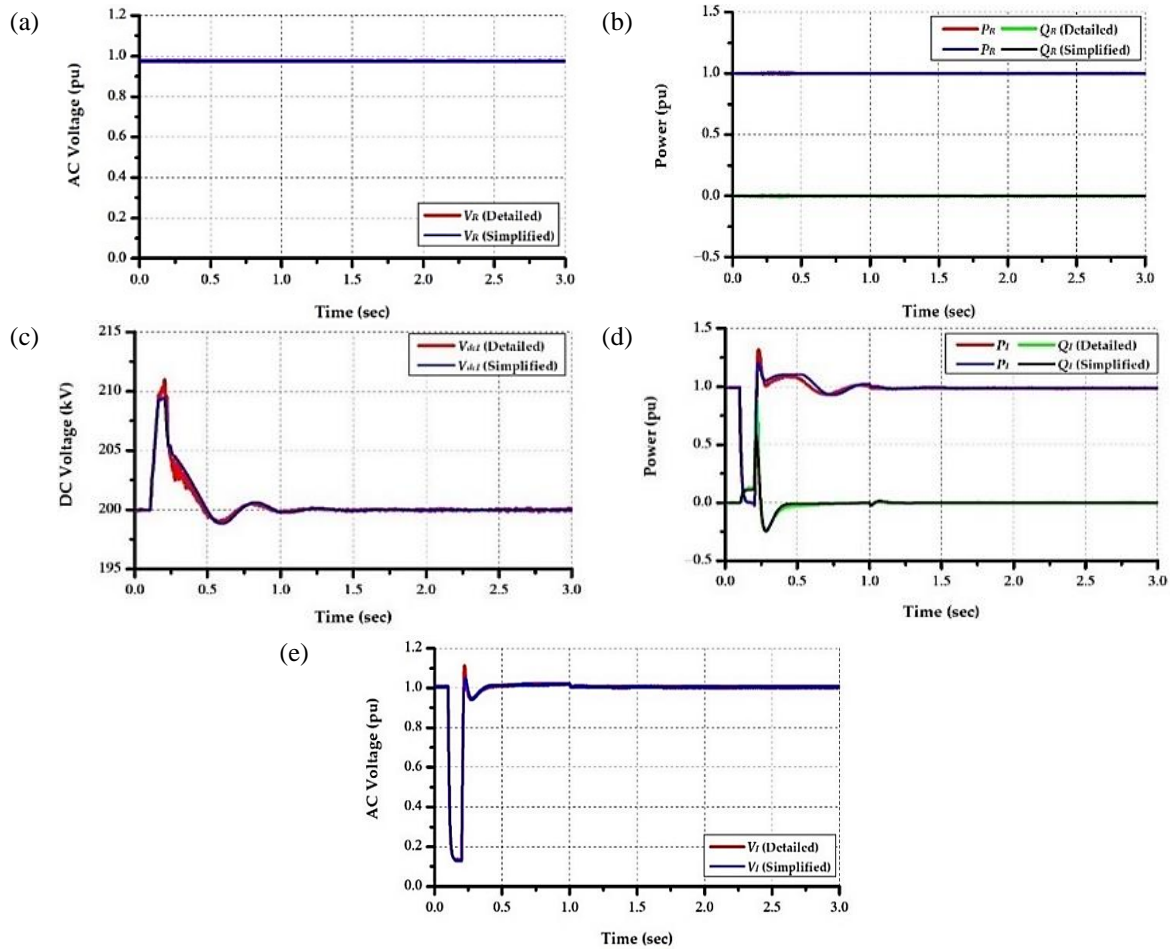


Figure 14. Simulation results of transient study for 3LHG: (a) AC voltage response at Bus B1, (b) active and reactive power responses at Bus B1, (c) DC voltage response at the transmission line, (d) active and reactive power responses at Bus B4, and (e) AC voltage response at Bus B4

## 6. CONCLUSION

In this paper, a simplified model design for an MMC-HVDC transmission system is presented. The PSCAD/EMTDC program was used to perform a comparison response analysis of the proposed simplified model and the detailed model in steady state and transient conditions to confirm the validity of the proposed simplified model. Ramp and step input signals are used in steady state analysis. In the transient analysis of an AC system, asymmetrical two lines to ground fault and symmetrical three lines to ground fault are considered disturbances. It is possible to verify that the simplified model is accurate enough. In addition, simulation time can be significantly reduced. The simplified model proposed here can be used to effectively analyze the dynamic properties of power systems such as MMC-HVDC transmission lines. In a future study, the authors intend to extend the proposed simplified model to analyze multi-area power systems with multiple HVDC transmission terminals.

## ACKNOWLEDGEMENTS

The authors would like to thank the Republic of Indonesia's Ministry of Research, Technology, and Higher Education for funding this research through the PDKN program.




## REFERENCES

- [1] N. R. Watson and J. D. Watson, "An overview of HVDC technology," *Energies*, vol. 13, no. 17, 2020, doi: 10.3390/en13174342.
- [2] W. G. Cigre, "CIGRE Working Group B4.72. DC grid benchmark models for system studies," *Technical Brochure 804*, no. 2020.
- [3] Siemens AG, "HVDC PLUS – the decisive step ahead," p. 16, 2016.
- [4] T. Hening, "State-of-the-art offshore power system in the German bight and technical mid-term expansion options," in *Proc. Offshore Wind R&D Conference 2015*, Bremerhaven, Germany, 13-15 Oct, 2015.
- [5] T. Tenne, "Energy: from sea to land," p. 18, 2020, [Online]. Available: [https://www.tenneet.eu/fileadmin/user\\_upload/Our\\_Grid/Offshore\\_Germany/2020\\_From\\_Sea\\_to\\_Land\\_Webversion.pdf](https://www.tenneet.eu/fileadmin/user_upload/Our_Grid/Offshore_Germany/2020_From_Sea_to_Land_Webversion.pdf).
- [6] S. Sato, T. Uchiumi, and A. Miura, "The construction of new Hokkaido-Honshu HVDC link project (B4-132)," *Cigre 2018*, 2018.




- [7] M. Mori, J. Chiba, A. Miura, K. Shimada, Y. Chiba, and D. Suzuki, "Functions and commissioning test of new Hokkaido-Honshu HVDC Link," in *Proc. CIGRE Paris 2020, B4-127*, 2020, pp. 1–8.
- [8] J. Qin, M. Saeedifard, A. Rockhill, and R. Zhou, "Hybrid design of modular multilevel converters for HVDC systems based on various submodule circuits," *IEEE Transactions on Power Delivery*, vol. 30, no. 1, pp. 385–394, 2015, doi: 10.1109/TPWRD.2014.2351794.
- [9] X. Shi, Z. Wang, B. Liu, Y. Liu, L. M. Tolbert, and F. Wang, "Characteristic investigation and control of a modular multilevel converter-based HVDC system under single-line-to-ground fault conditions," *IEEE Transactions on Power Electronics*, vol. 30, no. 1, pp. 408–421, 2015, doi: 10.1109/TPEL.2014.2323360.
- [10] S. Debnath, J. Qin, B. Bahrani, M. Saeedifard, and P. Barbosa, "Operation, control, and applications of the modular multilevel converter: A review," *IEEE Transactions on Power Electronics*, vol. 30, no. 1, pp. 37–53, 2015, doi: 10.1109/TPEL.2014.2309937.
- [11] A. Beddard, M. Barnes, and R. Preece, "Comparison of detailed modeling techniques for MMC employed on VSC-HVDC Schemes," *IEEE Transactions on Power Delivery*, vol. 30, no. 2, pp. 579–589, 2015, doi: 10.1109/TPWRD.2014.2325065.
- [12] S. P. Teeuwesen, "Simplified dynamic model of a voltage-sourced converter with modular multilevel converter design," *2009 IEEE/PES Power Systems Conference and Exposition, PSCE 2009*, 2009, doi: 10.1109/PSCE.2009.4839922.
- [13] D. Jovic and A. Jamshidi Far, "Phasor model of modular multilevel converter with circulating current suppression control," *IEEE Transactions on Power Delivery*, vol. 30, no. 4, pp. 1889–1897, 2015, doi: 10.1109/TPWRD.2014.2372780.
- [14] N. T. Trinh, M. Zeller, K. Wuerflinger, and I. Erlich, "Generic model of MMC-VSC-HVDC for interaction study with AC power system," *IEEE Transactions on Power Systems*, vol. 31, no. 1, pp. 27–34, 2016, doi: 10.1109/TPWRS.2015.2390416.
- [15] S. Liu, Z. Xu, W. Hua, G. Tang, and Y. Xue, "Electromechanical transient modeling of modular multilevel converter based multi-terminal HVDC systems," pp. 1–1, 2014, doi: 10.1109/pesgm.2014.6938791.
- [16] U. N. Gnanarathna, A. M. Gole, and R. P. Jayasinghe, "Efficient modeling of modular multilevel HVDC converters (MMC) on electromagnetic transient simulation programs," *IEEE Transactions on Power Delivery*, vol. 26, no. 1, pp. 316–324, 2011, doi: 10.1109/TPWRD.2010.2060737.
- [17] J. Peralta, H. Saad, S. Denneriere, J. Mahseredjian, and S. Nguefeu, "Detailed and averaged models for a 401-level MMC-HVDC system," pp. 1–1, 2013, doi: 10.1109/pesgm.2013.6672356.
- [18] H. Saad *et al.*, "Dynamic averaged and simplified models for MMC-based HVDC transmission systems," *IEEE Transactions on Power Delivery*, vol. 28, no. 3, pp. 1723–1730, 2013, doi: 10.1109/TPWRD.2013.2251912.
- [19] H. Saad *et al.*, "Modular multilevel converter models for electromagnetic transients," *IEEE Transactions on Power Delivery*, vol. 29, no. 3, pp. 1481–1489, 2014, doi: 10.1109/TPWRD.2013.2285633.
- [20] M. Rosyadi, A. Umemura, R. Takahashi, and J. Tamura, "Detailed and average models of a grid-connected MMC-controlled permanent magnet wind turbine generator," *Applied Sciences (Switzerland)*, vol. 12, no. 3, 2022, doi: 10.3390/app12031619.
- [21] CIGRE B4, "Guide for electromagnetic transient studies involving VSC converters," *Technical Brochure 832*, no. April, pp. 3–184, 2021.
- [22] M. Davies, M. Dommaschk, J. Dorn, J. Lang, D. Retzmann, and D. Soerangr, "HVDC PLUS-basics and principle of operation," *Siemens Energy Sector Report E T PS SL/DSoe/Re*, 2021.
- [23] D. Gamboa and A. Timofejevs, "Control of MMC in HVDC Applications," pp. 1–79, 2013.
- [24] W. Li, L. A. Gregoire and J. Belanger, "Control and performance of a modular multilevel converter system," *IEEE Bologna PowerTech Conference*, no. April, pp. 1–8, Halifax, Canada, 6-8 September, 2011. [Online]. Available: <http://citeseerx.ist.psu.edu/viewdoc/summary?doi=10.1.1.731.4484>.
- [25] Y. Wang, S. Liao, Q. Xu, L. Wang, and J. M. Guerrero, "Coordinated design of control parameters for improving interactive and internal stability of MMC-HVDC," *International Journal of Electrical Power and Energy Systems*, vol. 140, 2022, doi: 10.1016/j.ijepes.2022.108065.
- [26] Manitoba Hydro International, "PSCAD V5 Application Help," 2021, [Online]. Available: <https://www.pscad.com/webhelp-v5-ol/ol-help.htm>.
- [27] M. M. Belhaouane, M. Ayari, X. Guillaud, and N. B. Braiek, "Robust control design of MMC-HVDC systems using multivariable optimal guaranteed cost approach," *IEEE Transactions on Industry Applications*, vol. 55, no. 3, pp. 2952–2963, 2019, doi: 10.1109/TIA.2019.2900606.
- [28] I. El Myasse *et al.*, "Observer and nonlinear control design of Vsc-Hvdc transmission system," *SSRN Electronic Journal*, 2022, doi: 10.2139/ssrn.4126089.
- [29] Q. Tu, Z. Xu, and J. Zhang, "Circulating current suppressing controller in modular multilevel converter," *IECON Proceedings (Industrial Electronics Conference)*, pp. 3198–3202, 2010, doi: 10.1109/IECON.2010.5675048.
- [30] R. Darus, G. Konstantinou, J. Pou, S. Ceballos, and V. G. Agelidis, "Comparison of phase-shifted and level-shifted PWM in the modular multilevel converter," *2014 International Power Electronics Conference, IPEC-Hiroshima - ECCE Asia 2014*, pp. 3764–3770, 2014, doi: 10.1109/IPEC.2014.6870039.
- [31] L. G. Franquelo, J. Rodriguez, J. I. Leon, S. Kouro, R. Portillo, and M. A. M. Prats, "The age of multilevel converters arrives," *IEEE Industrial Electronics Magazine*, vol. 2, no. 2, pp. 28–39, 2008, doi: 10.1109/MIE.2008.923519.
- [32] IEC-62747, "Terminology for voltage-sourced converters (VSC) for high-voltage direct current (HVDC) systems," *International Electrotechnical Commission*, pp. 1–11, 2014.
- [33] G. Stamatou and Chalmers tekniska högskola. Department of Energy and Environment, "Analysis of VSC-based HVDC systems," 2016.

## BIOGRAPHIES OF AUTHORS






**Marwan Rosyadi**    is a researcher/educator in Department of Electrical Engineering, Faculty of Engineering, Universitas Muhammadiyah Surabaya, Indonesia. He received B. Eng degree in electrical engineering from Institut Teknologi Adhi Tama Surabaya (ITATS) in 2004, M. Eng degree in electrical engineering from Institut Teknologi Sepuluh Nopember (ITS) in 2006, and Dr. Eng. degree from Kitami Institute of Technology in 2013. His research interests are dynamic stability and control of power system integrated with wind turbine generator, solar PV, Battery Energy Storage, FACT devices, hydrogen generator, and HVDC transmission system. He can be contacted at email: [rosyadi@um-surabaya.ac.id](mailto:rosyadi@um-surabaya.ac.id).






**Atsushi Umemura**    received Dr. Eng. degree from Tokyo Denki University and joined Ohashi Engineering Co. Ltd. He became an Assistant Professor in the department of Electrical and Electronic Engineering, Kitami Institute of Technology in 2012, and has been an Associate Professor in the same department since 2020. His research interests include robotics, mechatronics, and power electronics. He can be contacted at email: umemura@mail.kitami-it.ac.jp.






**Rion Takahasi**    received the B.Sc. Eng. and Dr. Eng. Degrees from Kitami Institute of Technology, Japan, in 1998 and 2006 respectively, all in Electrical and Electronic Engineering. Now he is working as Associate Professor in Department of Electrical and Electronic Engineering, Kitami Institute of Technology. His major research interests include analysis of power system transient, FACTS and wind energy conversion system. He is a member of IEEE. He can be contacted at email: rtaka@mail.kitami-it.ac.jp






**Junji Tamura**    received his B. Sc. Eng. Degree from Muroran Institute of Technology, Japan, in 1979 and M.Sc. Eng. and Dr. Eng. degrees from Hokkaido University, Japan, in 1981 and 1984 respectively, all in electrical engineering. He became a lecturer in 1984, an Associate Professor in 1986, and a professor in 1996 at the Kitami Institute of Technology, Japan. Dr. Tamura is a Senior Member of the IEEE Power Engineering Society. He can be contacted at email: tamuraj@mail.kitami-it.ac.jp.






**Takanori Uchiumi**    received the B. Eng., M. Eng. and D. Eng. degrees from Muroran Institute of Technology, Japan, in 1995, 1997 and 2004 respectively, all in Electrical and Electronic Engineering. Now he works for Hokkaido Electric Power Network, Inc. as Manager of Power System Planning Section., Engineering Department. He can be contacted at email: t-uchi@epmail.hepco.co.jp.



**Masanori Mori**    received the B. Eng. and M. Eng. degrees from Muroran Institute of Technology, Japan, in 2001 and 2003 respectively, all in Electrical and Electronic Engineering. Now he works for Hokkaido Electric Power Network, Inc. as member of HVDC Interconnection Planning and Engineering Section., Engineering Department. He can be contacted at email: mori-m@epmail.hepco.co.jp.



**Hiroki Miyata**    received Dr. Eng. degree from Tokyo Denki University and joined Ohashi Engineering Co. Ltd. He became an Assistant Professor in the department of Electrical and Electronic Engineering, Kitami Institute of Technology in 2012, and has been an Associate Professor in the same department since 2020. His research interests include robotics, mechatronics, and power electronics. He can be contacted at email: umemura@mail.kitami-it.ac.jp.